



## Identification of early-age concrete temperatures and strains: Monitoring and numerical simulation

Miguel Azenha, Rui Faria \*, Denise Ferreira

LABEST-Laboratory for the Concrete Technology and Structural Behaviour, Faculdade de Engenharia da Universidade do Porto, Rua Dr. Roberto Frias, 4200-465 Porto, Portugal

### ARTICLE INFO

#### Article history:

Received 1 July 2008

Received in revised form 8 December 2008

Accepted 29 March 2009

Available online 8 April 2009

#### Keywords:

Cement hydration

Early-age concrete

Vibrating wire strain gages

Thermal cracking

Numerical simulation

### ABSTRACT

Concrete at early-ages experiences thermal deformations due to the heat generation caused by the cement hydration reactions. These deformations may lead to cracking of concrete, for which the use of numerical models in order to foresee and prevent this problem is of crucial importance. However, these numerical models must be appropriately validated by monitoring the young concrete behaviour. The conducted research regards an experimental work carried out with two main goals: (i) to evaluate the performance of different kinds of strain gages, in order to determine the more adequate ones for monitoring concrete deformations during early-ages after casting; (ii) to interpret the experimental measurements of temperatures and strains in concrete, by using a numerical model. Two different vibrating wire strain gages were used to measure early-age deformations in a concrete prism tested in the laboratory: one with a metallic housing and the other with a plastic one. The instant of solidarization of the sensors to concrete and the temperature sensitivity of their signals during the pre-solidarization period are key points as far as measurement of concrete early-age strains is concerned, which were examined for the present work. A thermo-mechanical numerical model was used to simulate the early-age concrete behaviour of the specimen. After a brief description of the model background, a comparison of the numerical predictions with the experimental results is made.

© 2009 Elsevier Ltd. All rights reserved.

### 1. Introduction

Early-age concrete behaviour is a problem of great concern nowadays, closely related to the increasing use of high performance concrete, where cracking may arise not only due to autogenous shrinkage, but also in result of deformations caused by the heat generated during the cement hydration reactions. Therefore, it is important to have numerical tools for predicting temperatures and stresses in early-age concrete, in order to foresee – and if possible to avoid – premature cracking of thermal origin. The thermo-mechanical methodology used in this paper is based on the Finite Element Method (FEM), and it accomplishes a thermal analysis, followed by a mechanical one. The thermal analysis assimilates the heat of the cement hydration as an internal heat source, and it accounts for the energetic flows by convection and radiation between concrete and the environment. As far as the mechanical analysis is concerned, the evolution of concrete mechanical properties, as well as the influence of creep, are considered.

In this regard, it is essential to develop suitable monitoring practices for evaluating temperatures and strains in early-age concrete, so as to validate the numerical models. As during early-ages concrete has evolving mechanical properties, there are difficulties

related to measurement of strains, while concrete stiffness and temperature vary significantly and are largely amplified as compared to the final hardened stage. Doubts about the adequacy of using strain sensors developed for hardened concrete in early-age measurements still persist, based on two main concerns: the instant of solidarization of the sensor to concrete is difficult to determine, and the temperature sensitivity of the strain sensor when embedded into a material ranging from a liquid to a solid state can only be roughly estimated. Solidarization of the strain sensors to concrete is a fundamental dilemma within the early-age monitoring context, depending mostly on the ratio of stiffnesses between the concrete and the sensor. Solidarization is here defined to occur when the strain gage is capable of reproducing variations in concrete deformations, which is only foreseeable when concrete stiffness is sufficiently high to ensure the sensor to be perfectly attached.

Electrical strain gages with ceramic insulation have wide spread usage among large-scale applications on civil engineering, due to their economy and sturdiness. Nevertheless, for early-age strain measurements these resistive electrical sensors revealed some problems [1]. One of the main reasons for this inadequacy is that these sensors are made from a material with the same thermal dilation coefficient of hardened concrete, in order to perform an “auto compensation” of concrete thermal deformation. Another problem with these sensors, and based on the authors’ experience,

\* Corresponding author. Tel.: +351 22 508 1950; fax: +351 22 508 1835.  
E-mail address: [rfaria@fe.up.pt](mailto:rfaria@fe.up.pt) (R. Faria).

is that the existence of electrical apparatus in the sensors vicinity may cause current peaks that interfere with the signals, being this an important problem when monitoring campaigns are to be performed on real site constructions.

On the other hand, vibrating wire strain gages embedded in hardened concrete require temperature compensation procedures that strictly depend on the thermal dilation coefficient of the wire placed internally, which is constant and known.

Few references were found on the theme of concrete strain monitoring at early-ages. Even so, some practical applications concerning in-field early measurements are reported in the literature. An overview of field measurement techniques and data analyses on early-age concrete structures is acutely discussed by Cusson [2]. Concerning field applications, Anson and Rowlinson [3] reported the use of vibrating wire strain gages in early-age strain measurements in concrete tank walls, which were successful only when the internal temperature stabilized. Another application reported by Heimdal et al. [4] regards a concrete box culvert in Norway, instrumented with embedded vibrating wire strain sensors and electrical strain gages, where reliable results were obtained after the age of 15 h. Morabito [5] reports an early-age concrete monitoring application on a dam sluice gate, in which embedded vibrating wire strain gages and electrical strain gages welded to the reinforcement were used, revealing that along the heating and cooling periods of cement hydration measurements from both types of sensors were quite dissimilar, although following similar tendencies from then on. Temperature measurements during the concrete curing of the viaduct deck of the Öresund Link are reported in Cervera et al. [6], where cracking risk scenarios are analyzed with a thermo-mechanical model. Also, Azenha and Faria [7] reported a case study of a reinforced concrete foundation of a wind tower, where temperatures and stresses due to cement hydration were evaluated. As far as laboratory experimental work is concerned, O'Moore et al. [8] have used vibrating wire strain gages with a plastic housing on early-age monitoring of industrial pavements, reporting that incoherent measurements of strains were obtained at the very early-ages.

More recently, optical fibre technology is reported to be a good solution in early-age concrete temperature and strain measurements, because of its high precision and resolution, insensitivity to electromagnetic fields and mechanical robustness [9–12]. In terms of in-field applications, this technology was used by Glisic and Inaudi [13] for monitoring temperatures and deformations in early-age concrete cast above a hardened element, and in composite steel-concrete structures during cement hydration [14].

All the above cited works report difficulties in identifying concrete strains during the heating phase of cement hydration, approximately around the first 12–15 h after casting. When the cooling phase commences, the output signals from different strain gage sensors start to have consistent and similar evolutions.

Based on the experience of the authors of this paper, the major difficulty on early-age concrete monitoring relates also to measurement of strains [1,15]. Inadequacy of most of the standard strain gages for this early stage of concrete, where high variations of temperature and stiffness are present, adding up to problems of characterizing the developing material, are the main causes of the unsuccessful strain monitoring during the cement hydration of concrete. The key issues that persist are: (i) the instant of solidarization of the sensor to concrete and (ii) the thermal sensitivity of the strain gage before and after the solidarization.

In this paper a laboratory campaign was performed on a concrete prism, and had the following two goals:

- To evaluate the performance of different types of strain gages. One of the kinds of sensors selected for this research was the vibrating wire strain gage with a metallic casing,

because of its robustness for *in situ* applications (where mechanical injuries due to concrete vibrators are frequent). In order to identify the instant of solidarization to concrete of this metallic housed strain gage, a vibrating wire strain gage with a plastic (and thus less stiff) casing was also used.

- To use a thermo-mechanical numerical model as a tool for better interpreting the experimental results, taking advantage of the temperatures and strains measured at various points of the concrete prism during the cement hydration stage.

In this experimental work, detailed in Section 2, concrete deformations refer to 'total strains', that is, the sum of the 'mechanical' and 'thermal' components.

An additional important outcome of this study is to support the determination of stresses in early-age concrete, in order to compare the maximum principal tensile stresses with the evolving tensile strengths, and finally to predict the cracking risk in concrete. This is accomplished by using a thermo-mechanical model, briefly outlined in Section 3, and applied to the above-referenced concrete prism in Section 4.

## 2. Experimental campaign on a prismatic concrete specimen

### 2.1. Geometry, materials and monitoring

An experimental monitoring campaign for measuring early-age temperatures and strains on a concrete prism was carried out, fulfilling the following requisites: (i) the prism should have geometry allowing for an easy and accurate numerical discretization, with dimensions compatible with the laboratory work, and (ii) at the same time it should engender a heat generation potential high enough to cause significant temperature and strain gradients. The geometry of the concrete prism, whose dimensions are  $0.60 \times 0.30 \times 0.60 \text{ m}^3$ , is presented in Fig. 1. Lateral faces and base of the element were insulated with 6 cm thick polystyrene plates and 2.1 cm thick plywood formworks. The mix composition of the concrete was as follows:  $1134 \text{ kg m}^{-3}$  of calcareous gravel,  $263 \text{ kg m}^{-3}$  of recycled concrete sand,  $264 \text{ kg m}^{-3}$  of natural sand,  $400 \text{ kg m}^{-3}$  of cement type I 42.5R and  $200 \text{ kg m}^{-3}$  of water. Concrete casting and the experimental procedures took place inside a climatic chamber with a constant temperature  $T = 20^\circ\text{C}$  and relative humidity  $RH = 50\%$ ; data acquisition started at the end of the casting operations.

Regarding the experimental monitoring measurements, different types of sensors were placed at symmetrical positions in relation to plane B-B' of Fig. 1, where identical temperatures and strains are to be expected, in order to compare their measurements, performances and aptitudes. Concerning the temperature sensors, two types were adopted: the thermocouple type K (TC), very easy to use and economical, but with a low precision of  $\pm 2.2^\circ\text{C}$ , and resistive temperature sensors (PT100), housed with a material with high thermal conductivity (copper), with a high precision of  $\pm 0.1^\circ\text{C}$ . As far as the strain sensors are concerned, two types of vibrating wire strain gages with rather dissimilar casings were used: one with a metallic and stiffer housing (VWM) and the other with a plastic and less stiff casing (VWP). Vibrating wire strain gages have internal resistive temperature sensors, so they are able to monitor strains and temperatures at the same time and location. All these strain gages were embedded into concrete.

Sensor locations are schematically represented in Fig. 1. Temperature sensors were placed in the lateral faces and base of the concrete prism, as well as between polystyrene layers, in order to validate the thermal boundary conditions of the numerical model; in the concrete element itself 16 TC and 2 PT100 were placed at

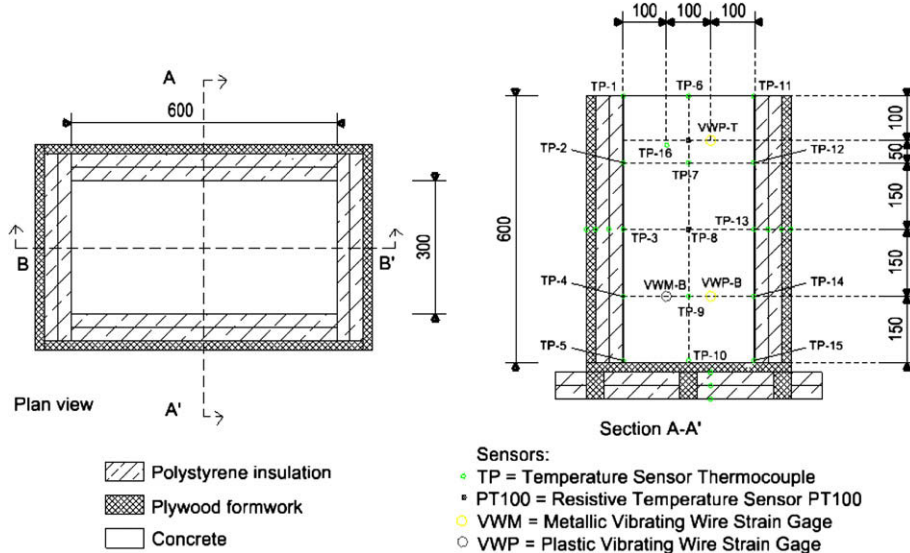


**Fig. 1.** Experimental set-up: concrete and sensors location.

different heights. The experimental set-up, reproduced also in Fig. 2, includes the following strain sensors located at two levels along the height: (i) on the top level (0.10 m from the top surface), the VWP-T was sited; (ii) on the bottom level, 0.15 m above the base, the vibrating wire strain gages VWM-B and VWP-B were placed (Fig. 2b). These nomenclatures of “top” (-T) and “bottom” (-B) levels will also be used later on this paper, for the discussion of experimental and numerical results.

One should be aware that the thermal deformation of the vibrating wire ( $11 \mu\text{e K}^{-1}$ , according to the manufacturer's specification) must be withdrawn from the gage response to reflect the sensor total deformation. All the strain measurements reported in this paper have been previously corrected for this effect of thermal dilation of the vibrating wire.

In addition, a preliminary experiment was carried out to compare the responses of the two types of vibrating wire strain gages when subjected to temperature variations in free regime, that is, not embedded into concrete. These responses reflect the free thermal deformations of the sensor casings, which is a relevant information concerning the interpretation of the sensor output prior to solidarization to concrete. The strain gages with the plastic and metallic casings were placed inside a climatic chamber with prescribed temperature variations. The corresponding responses were  $46.24 \mu\text{e K}^{-1}$  for sensor VWP and  $4.55 \mu\text{e K}^{-1}$  for sensor VWM, showing clearly that sensor VWP has much higher temper-

ature sensitivity than VWM. Nevertheless, when these strain gages are embedded into hardened concrete, the response to equal temperature variations must be the same, as total strains are prescribed by the concrete deformation.

## 2.2. Discussion of the experimental results

### 2.2.1. Temperatures

Temperatures measured in the concrete prism by the temperature sensors integrated on the vibrating wire strain gages are presented in Fig. 3. One can notice that, as expected, the sensors on the bottom level recorded higher temperatures ( $64^\circ\text{C}$ , at the age of 17 h) than the one on the top level ( $55^\circ\text{C}$  at 11 h). It is also important to note the high coincidence of the responses of the two bottom level sensors VWM-B and VWP-B. In Fig. 3 it can also be noticed that the heating period begins right after the concrete placement, and lasts for about 20 h; it is then followed by the cooling period, and after 160 h thermal equilibrium is reached between the concrete element and the climatic chamber environment.

In Fig. 4 measurements from the TP thermocouples placed along the lateral boundaries of Fig. 1 are presented. One can straightforwardly observe the thermal insulation influence of the polystyrene placed on the lateral and bottom faces: as it was expected, the areas near the non-insulated top surface reached lower temperatures. It is also worth noting the strong coherence of temperatures

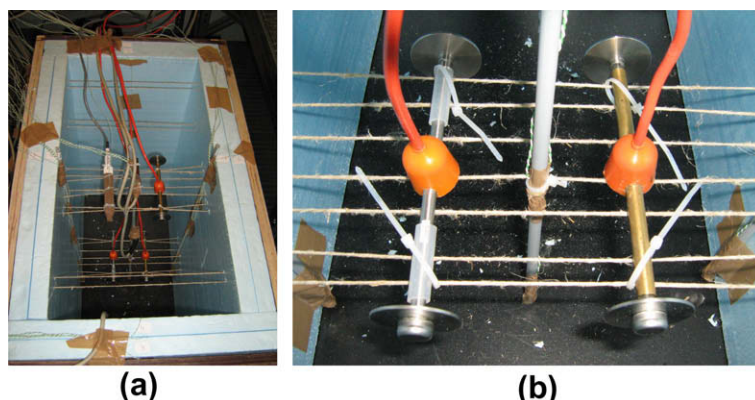


**Fig. 2.** (a) Overview of polystyrene insulation and sensors and (b) VWM-B and VWP-B.

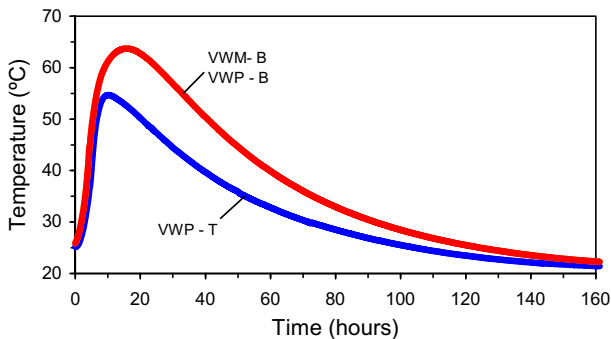


Fig. 3. Temperatures measured on the vibrating wire strain gages.

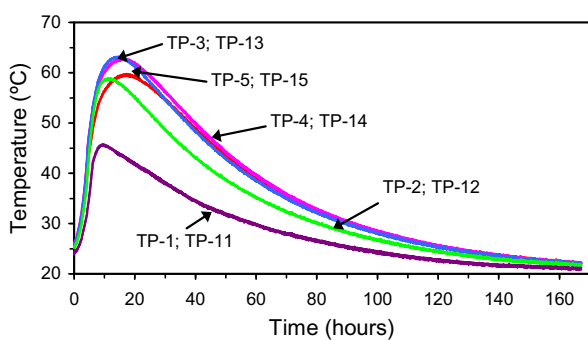


Fig. 4. Temperatures measured by the thermocouples on the lateral boundaries.

measured by the TP placed symmetrical along the two vertical boundaries (TP1 and TP11, TP2 and TP12 and so on up to TP5 and TP15) of the concrete element (see Fig. 1 for identification of sensors location).

## 2.2.2. Total strains

Fig. 5 reproduces the total strains measured by the various sensors embedded in the concrete element: VWM-B and VWP-B at the bottom level; VWP-T at the top level. The expectable tendency that the total strains were superior at the bottom level (because it reached higher temperatures that led to larger expansions) than at the top level was confirmed by the VWP-T and VWP-B curves in Fig. 5.

Focusing on the bottom level, the strain gages recorded different peak expansions (see Fig. 5), which can have two main

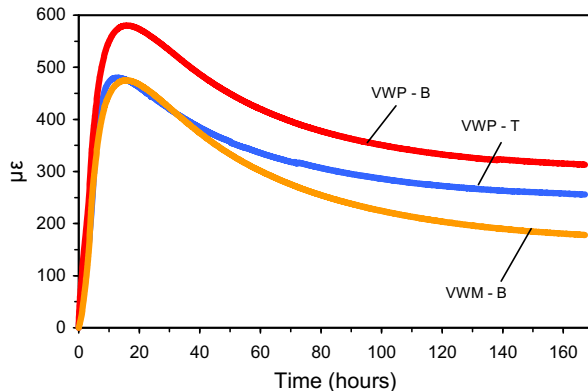


Fig. 5. Total strains measured in concrete.

sources: (i) VWP-B stiffness is much lesser than that of VWM-B, thus solidarization of the plastic sensor to the early-age concrete occurs before than for the metallic one, engendering higher final deformations on sensor VWP-B; (ii) before solidarization to concrete sensor VWP-B reveals a greater sensitivity to temperature variations than VWM-B (according to the free regime characterization mentioned in Section 2), therefore recording higher thermal deformations at the heating phase. During the concrete cooling phase, after the age of 20 h, both strain gages present identical evolution tendencies. Hence, it is interesting to notice that both types of vibrating wire strain gages are adequate to measure strains during the concrete cooling phase, a stage where this material already presents a reasonable stiffness, assuring a perfect solidarization to both types of sensors. These results are coherent with previous findings reported in the literature [3–5,8].

Bearing in mind that the low stiffness of the plastic vibrating wire strain gages allows them to solidarize to concrete sooner than the metallic ones, that instant of solidarization may be defined, in a simplified way, as the one when the response evolutions for both strain gages exhibit the same trends. In Fig. 6 a detail of the strains recorded by both types of vibrating wire strain gages (VWP-B and VWM-B) until the age of 4 h is represented, where the plastic sensor graph was vertically translated until its peak became coincident with the one related to the metallic sensor; temperature evolution for the location of these strain sensors is also represented. Concerning the plastic sensor, one can notice a change on the derivative sign of the evolution trend signal at the age of 0.83 h, being reasonable to consider this the instant of solidarization of sensor VWM-B to concrete. It is also possible to observe that beyond approximately 2.3 h both the metallic and the plastic vibrating wire strain gages provide the same total strains, corresponding that instant to the one at which the metallic sensor solidarizes to concrete. With reference to the temperature variations ( $\Delta T$ ) that the vibrating wire strain gages experienced between the instant of concrete placement and the instant of solidarization, it can be remarked that: (i) the plastic strain gage was subjected to  $\Delta T = 1.5^\circ\text{C}$ , which corresponds to a free thermal deformation of the sensor casing of about  $69 \mu\text{e}$ ; (ii) the metallic strain gage experienced a  $\Delta T = 5.7^\circ\text{C}$ , which corresponds to a free thermal deformation of  $26 \mu\text{e}$  for the sensor casing. This thermal sensitivity values are merely indicative of the difference between the two types of vibrating wire strain gages, since in the pre-solidarization phase the sensor casings are not totally free to deform thermally.

As the solidarization instant for a metallic vibrating wire strain gage was already determined (though approximately), it is possible to adjust the corresponding signal of measured strain by vertically

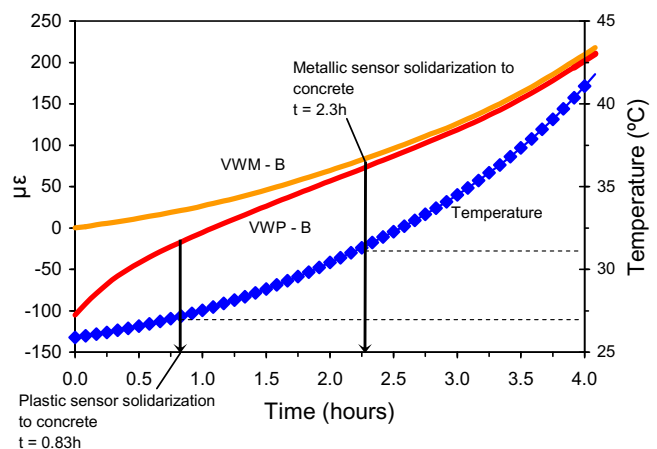


Fig. 6. Solidarization instants of the plastic and metallic vibrating wire strain gages.

shifting the graph, so as to cancel the deformations registered prior to solidarization (see Fig. 7). In this way, the original signal of VWM-B may be considered as an upper-bound of the true total strains in concrete, and the corrected graph a lower-bound. It is important to remark that the upper-bound can be erroneous if the concrete total deformations that took place in the pre-solidarization period are greater than the recorded sensor temperature sensitivity. Nonetheless, it can be considered that the real concrete total strains should lie within the interval defined by the upper- and lower-bounds in Fig. 7: in one hand the upper-bound possibly will overestimate the concrete total strains, due to the gage sensitivity to the temperature variations that occurred prior to solidarization; and in the other hand the lower-bound does not consider the total strains that occurred in concrete during the interval while solidarization evolves. In comparison to the plastic housed strain gage, the lesser thermal sensitivity of the metallic cased sensor during the period prior to full solidarization is an interesting feature in what concerns measurements of early-age concrete strains, in spite of a later solidarization. Nevertheless, plastic vibrating wire strain gages are quite useful for the definition of the instant of solidarization of the metallic housed sensors.

### 3. Thermo-mechanical model

The following heat diffusion equation based on the Fourier's Law expresses the early-age concrete transient heat conduction

$$k\nabla \cdot (\nabla T) + \dot{Q} = \rho c \dot{T} \quad (1)$$

where  $k$  and  $\rho c$  are the thermal conductivity and the volumetric specific heat of concrete, respectively,  $T$  is the temperature and  $Q$  is the internal heat generation due to the cement hydration. The rate of internal heat generation may be considered by an expression based on the Arrhenius Law [16]

$$\dot{Q} = A f(\alpha) e^{-E_a/(RT)} \quad (2)$$

where  $E_a$  is the apparent activation energy,  $A$  is a rate constant,  $f(\alpha)$  is a normalized function for heat,  $R = 8.314 \text{ J mol}^{-1} \text{ K}^{-1}$  is the Boltzmann's constant, and variable  $\alpha$  expresses the degree of advancement of the cement hydration reaction, here computed as the ratio between the heat released up to the current time and the total heat expected to be liberated upon completion of hydration ( $Q_\infty$ ).

Concerning the mechanical problem, the concrete properties evolution as a result of cement hydration can be quantified accordingly to the Maturity Method [17], directly related to the Equivalent Age Concept, which allows to convert the real age of concrete  $t$  (in days) in an equivalent age  $t_{eq}$  (also in days):

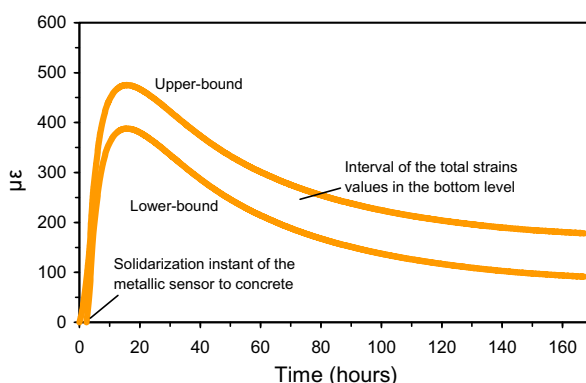


Fig. 7. Responses on sensor VWM-B: upper-bound (original graph) versus lower-bound (after signal deletion until solidarization to concrete).

$$t_{eq} = \int_0^t e^{-\frac{E_a}{R} \left( \frac{1}{T(\tau)} - \frac{1}{T_{ref}} \right)} d\tau \quad (3)$$

The equivalent age is superior to the real age if the temperature history  $T(\tau)$  during hydration is greater than the reference temperature (normally  $T_{ref} = 20^\circ\text{C}$  in European countries). In this manner, it is possible to account for the accelerating role of the curing temperature on the evolution of the concrete mechanical properties. To account for the evolution of the concrete elastic modulus  $E_{cm}$  during cement hydration, the following Eurocode 2 (EC2) [18] expression was adopted:

$$E_{cm}(t_{eq}) = e^{0.3s(1-\sqrt{28/t_{eq}})} E_{cm}(28) \quad (4)$$

where  $t_{eq}$  is defined by Eq. (3),  $E_{cm}(28)$  is the elastic modulus of concrete at the age of 28 days, and  $s$  is a parameter that accounts for the setting speed of the cement type used. The thermal dilation coefficient  $\alpha_T$  and the Poisson's ratio  $\nu$  of concrete were assumed to be constant during hydration, with the typical values of hardened concrete.

Regarding the viscoelastic behaviour of concrete during the early-ages, the Double Power Law (DPL) [19] has been used successfully in the numerical prediction of early-age stresses by de Borst and Van den Boogaard [20], where explicit comparisons between experiments and simulations revealed good coherence. More recently, extensive experimental campaigns devoted to compressive and tensile creep behaviour of concrete at early-ages [21,22] have shown good fits of the DPL to experimentally obtained creep curves, using either constant loading tests or experiments with concrete cast in TSTM restraining frames. Furthermore, it has been acknowledged by Bazant and Prasannan [23] that the DPL itself constitutes a particular case of the Solidification Theory for small creep durations. Therefore, it is considered that the use of the DPL is reasonable for the application of the present paper, and it was adopted by considering the following creep compliance function at time  $t$  for a load applied at instant  $t'$  (both times expressed in days):

$$J(t, t') = \frac{1}{E_0(t')} + \frac{\phi_1}{E_0(t')} (t')^{-m} (t - t')^n \quad (5)$$

where  $E_0(t')$  is the asymptotic elastic modulus (corresponding to short term loads), and  $\phi_1$ ,  $m$  and  $n$  are material parameters, calibrated based on experimental creep tests.

The numerical model briefly described is implemented in the FEM computational code DIANA (for further details see [1]), allowing to evaluate temperatures and stresses generated in concrete during the early-ages.

### 4. Interpretation of the experimental results with the numerical model

#### 4.1. Overview

The concrete prism monitored during the experimental campaign described in Section 2 was discretized with 3D finite elements (FE). Fig. 8 illustrates the double symmetry adopted in the numerical model, as well as the assumed thermal boundary conditions. As far as the model geometry is concerned, the following considerations are presented:

- Both the polystyrene insulations and the concrete were explicitly discretized with FE, and modelled according to their corresponding thermal and mechanical properties.
- Between the external boundaries and the environment a convection-radiation coefficient equal to  $10 \text{ W m}^{-2} \text{ K}^{-1}$  was considered, reproducing a stagnant air condition [1].

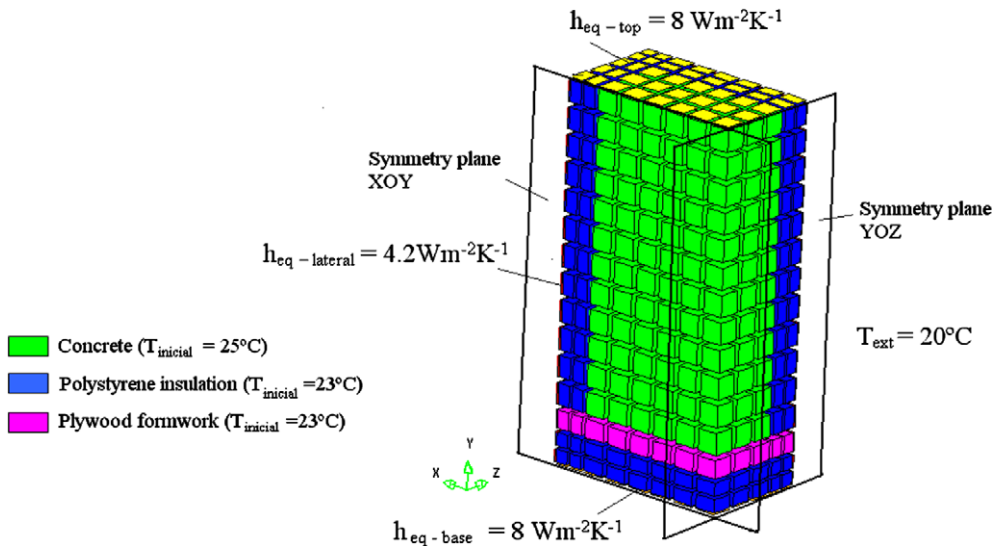


Fig. 8. Concrete prism: mesh, symmetries and thermal boundaries.

Solar radiation was disregarded, as the experiment occurred indoors, on a climatic chamber. The initial temperature of concrete during the casting operations was considered to be 25 °C, in correspondence to the first temperature measurements.

- The plywood formwork was simulated in two distinct ways: (i) at the vertical faces via an equivalent convection-radiation coefficient  $h_{eq} = 4.2 \text{ W m}^{-2} \text{ K}^{-1}$ , reproducing the heat flux to environment [1,24]; (ii) at the base, and since the formwork was placed between the concrete and the insulation, it was explicitly discretized with FE.

Regarding the mechanical boundary conditions, the following displacements were assumed to be null (see Fig. 8): (i) along direction  $X$  on the symmetry plane  $Y-O-Z$ , (ii) along direction  $Z$  on the symmetry plane  $X-O-Y$  and (iii) along direction  $Y$  on the bottom plane. As there is no relevant mechanical adherence between the concrete and the insulation or the formwork, mechanical properties of the polystyrene and plywood were considered negligible.

In regard to the thermal model for the concrete prism, the thermal properties considered for each material were the following: (i) concrete:  $k = 2.6 \text{ W m}^{-1} \text{ K}^{-1}$  and  $\rho c = 2.4 \times 10^6 \text{ J m}^{-3} \text{ K}^{-1}$ ; (ii) polystyrene:  $k = 0.035 \text{ W m}^{-1} \text{ K}^{-1}$  and  $\rho c = 2.84 \times 10^4 \text{ J m}^{-3} \text{ K}^{-1}$  and (iii) plywood:  $k = 0.15 \text{ W m}^{-1} \text{ K}^{-1}$  and  $\rho c = 8.544 \times 10^5 \text{ J m}^{-3} \text{ K}^{-1}$ . The Arrhenius Law expressed in Eq. (2) was determined through isothermal calorimetry [25–27], and the results from the tests performed at the isothermal temperatures of 20 °C, 30 °C, 40 °C, 50 °C and 60 °C allowed to determine the following parameters for the volumetric heat generation of the used concrete mix:  $E_a = 44.71 \text{ kJ mol}^{-1}$ ,  $A = 1.2066 \times 10^{11} \text{ W m}^{-3}$ ,  $Q_\infty = 1.43121 \times 10^8 \text{ J m}^{-3}$  and function  $f(x)$  characterized by the following set of data  $[x; f(x)] = [0; 0], [0.04; 0.569], [0.08; 0.824], [0.1; 0.904], [0.12; 0.957], [0.16; 0.999], [0.26; 0.926], [0.36; 0.732], [0.5; 0.415], [0.6; 0.245], [0.7; 0.131], [0.8; 0.065], [1; 0]$ .

Concerning the concrete mechanical characterization, compressive tests at the ages of one and three days were performed in order to obtain the following creep function coefficients (Eq. (5)):  $\phi_1 = 0.6$ ,  $m = 0.15$  and  $n = 0.20$ ; the  $E_0$  values were assumed to be 40% greater than the static elastic modulus at each age of loading. For defining the concrete elastic modulus  $E_{cm}$ (28), compressive tests were performed at the age of 28 days, resulting on the value of 39 GPa. Parameter  $s$  was considered to be 0.2, and the thermal dilation coefficient was taken as  $\alpha_T = 8 \times 10^{-6}$ , corresponding to a

volumetric weighted average of the thermal dilation coefficients of the concrete mix components [28,29]; Poisson's coefficient was assumed as  $\nu = 0.20$ . In the time window concerned with this early-age study of concrete (less than seven days) drying shrinkage was negligible, and so it was disregarded in the numerical model. However, autogenous shrinkage played an important role on the concrete early-age strains, and accordingly it was measured on a  $0.15 \times 0.15 \times 0.60 \text{ m}^3$  prismatic specimen, free to deform but insulated against moisture variations with paraffin, rendering the evolution curve depicted in Fig. 9.

With reference to the thermal analysis, the mesh presented in Fig. 8 corresponds to prismatic eight-noded FE with a  $2 \times 2 \times 2$  Lobatto integration scheme, whereas for the mechanical problem 20-noded FE with  $3 \times 3 \times 3$  Gauss points were adopted (both types of FE have coinciding corner nodes). The thermo-mechanical analysis was carried out until the age of seven days, with a time-step of 0.25 h.

#### 4.2. Temperatures

The temperatures obtained in the numerical simulation of the concrete prism will be compared to the experimental results presented in Section 2. Distribution of temperatures at the instant when the maximum was reached (15.8 h) is reproduced in

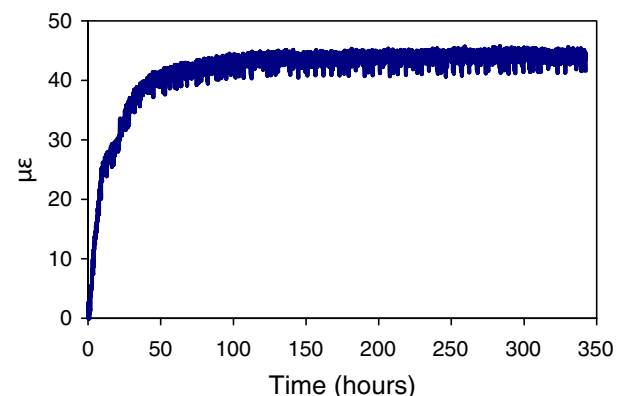
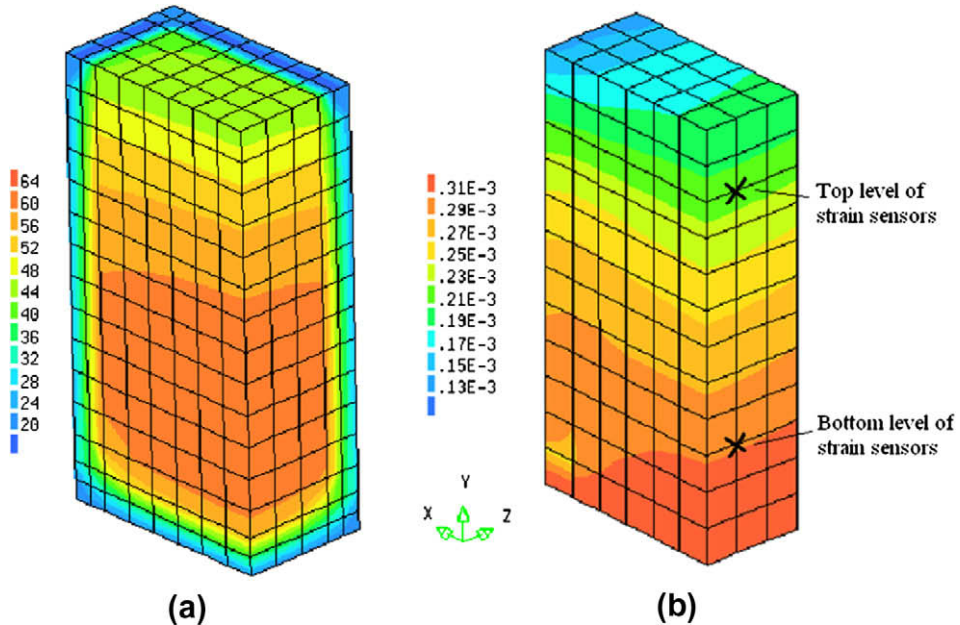


Fig. 9. Concrete free autogenous shrinkage evolution.



**Fig. 10.** Numerical results at the age of 15.8 h: (a) temperatures ( $^{\circ}$ C) and (b) total strains  $\varepsilon_x$ .

**Fig. 10a**, showing a significant coherence to the sensors measurements (see Fig. 4 for comparison).

Relating to the temperatures on the strain sensors, a direct comparison between the experimental measurements and the numerical results obtained throughout time is represented in Fig. 11. In addition, and to check the adequacy of the presumed boundary conditions on the thermal simulation, the numerical and experimental temperatures on the interfaces close to the vertical boundaries are presented in Fig. 12. In both figures a very good agreement between the numerical and experimental results can be observed, which validates the assumed simulation hypotheses.

#### 4.3. Total strains

Since the thermal model was well succeeded, there is some confidence to go into the mechanical problem. Accordingly, disagreements on the numerical total strains in relation to the experimental ones are to be considered due to insufficiencies of the mechanical model, or misinterpretation of the monitoring results.

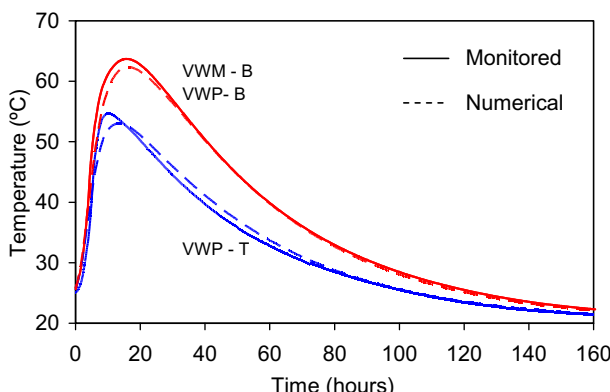


**Fig. 11.** Temperatures on the strain sensors.

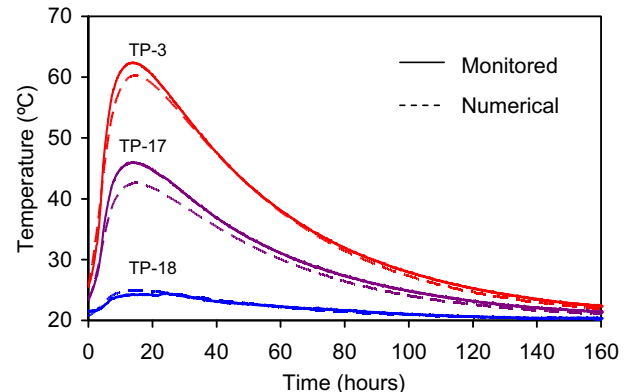


**Fig. 12.** Temperatures on several interfaces close to the vertical boundaries.

Adopting the same strategy as for the thermal analysis, numerical and experimental early-age concrete total strains will be compared. Concrete total strains  $\varepsilon_x$  computed numerically for the instant of maximum temperature (15.8 h) are presented in Fig. 10b. Is it interesting to notice the strain gradients between the top and bottom areas of the concrete prism, in correspondence to the two levels of strain sensors, and already identified on the experimental results discussion presented in Section 2.2. As far as the computed concrete tensile stresses are concerned, they remained always below the threshold of 0.5 MPa, pointing to an almost negligible cracking risk, which is consistent with the strain gages measurements (otherwise their graphs would have to show sudden hops).

Comparison of the total strains measured experimentally and the corresponding numerical predictions is made in Fig. 13, for both top and bottom levels of strain gages: discrepancies on the numerical strain peak values in relation to the experimental results are observed. However, and as previously remarked, results obtained directly from the vibrating wire strain gages are upper-bounds of the real total strains. After performing the vertical correction of the vibrating wire strain gages signals, as described for Figs. 6 and 7, the expectable total strains interval for the bottom

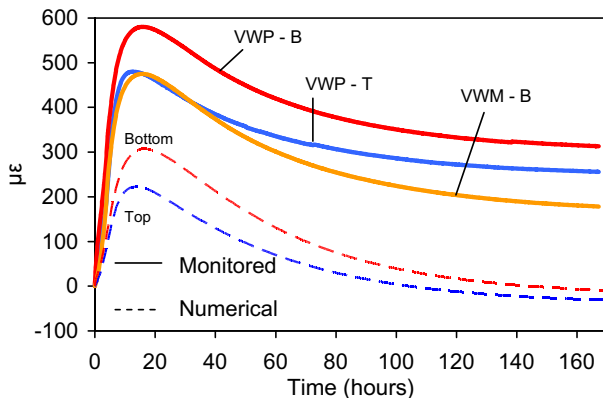


Fig. 13. Numerical and monitored total strains  $\varepsilon_x$ .

level sensors and the corresponding numerical results are depicted in Fig. 14: it is straightforwardly noticeable that although the numerical peak value is fairly under the assigned interval, evolution of the numerical curve is significantly similar to the ones from the monitoring campaign. Consequently, and within the normal errors acceptable for this kind of applications, it can be remarked that during the post-peak phase the numerical model provides high coherent evolutions of concrete total strains, when compared to the experimental ones.

Among the many reasons that may explain the differences on the peak total strains obtained from the experimental campaign or from the numerical model, one could refer to the following:

- Incorrectness of the assumed early  $E_{cm}$  evolution might be plausibly argued as leading to misleading results. Yet, in the present paper evolution of the elastic modulus of concrete was numerically simulated by using its corresponding expression in EC2, which is clearly not devised for very early-age stiffness evolutions, nor does it contemplate the dormant stage during which concrete stiffness should be considered as zero. Besides, recently a new method for monitoring the early-age concrete stiffness (right after casting) has been devised at the Faculty of Engineering of the University of Porto [30], and it is under a patenting process. The results obtained with this method for a very similar concrete to the one used in this application (same cement type and content) allowed a realistic early  $E_{cm}$  curve to be obtained, which was only significantly different from the EC2 one during the first few hours after casting. The use of that realistic  $E_{cm}$  curve on the numerical model for the present application yielded almost the same strains as the one from EC2. The reason

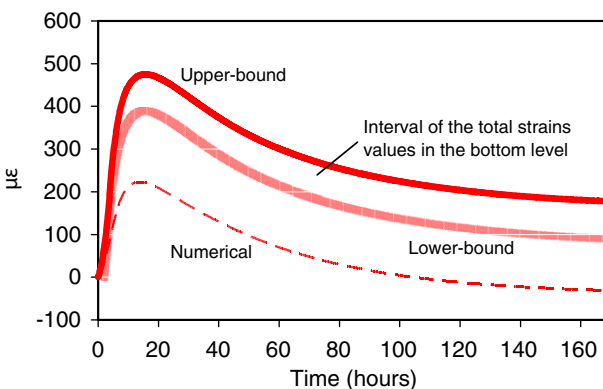


Fig. 14. Total strains  $\varepsilon_x$  at the lower level.

for this is that the temperatures that develop within the concrete prism are relatively uniform (see Fig. 10a), and the restraints induced by neighbouring parts of the prism at different temperatures are relatively small. Thus, as there is no external restraint to the deformation, and the internal restraint is relatively small, influence of changing the concrete elastic modulus is negligible given the fact that deformations are being commanded by thermal dilation (almost as if this was the case of free thermal dilation, which is clearly independent of the material stiffness, provided that no restraints are present).

- Insufficiencies of the creep model with regard to the viscoelastic behaviour of concrete could also be argued to be the reason for the observed discrepancies. Nonetheless, according to what has been stated above, as stiffness evolution of concrete seems to have small effect in this thermal dilation driven phenomenon, so does creep. The small influence of creep modelling was confirmed by conducting parametric analyses with dramatic changes in the creep laws (doubling and halving all parameters of the DPL), which led to negligible changes in the computed strains of the application envisaged in this paper.
- In regard to the strains calculations, the remaining mechanical parameter that might be responsible for the observed differences was the thermal dilation coefficient  $\alpha_T$ , which is not constant during the cement hydration process, as for simplification it was assumed in the present simulation, furthermore being also a property of rather complex experimental characterization. Evolution curves for  $\alpha_T$  with the equivalent age of concrete are shown in Fig. 15 [31–34]: the discrepancy is notorious, not only because of the differences on the analyzed concretes, but

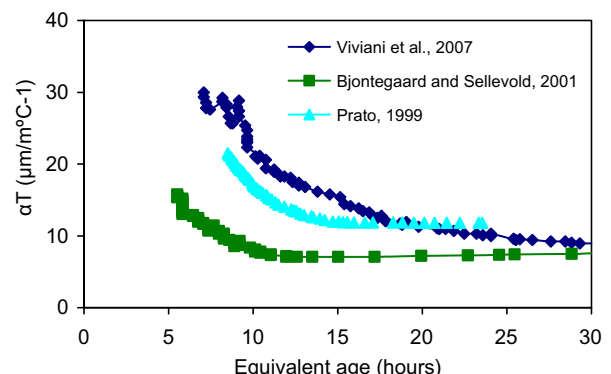


Fig. 15. Concrete thermal dilation coefficient during cement hydration.

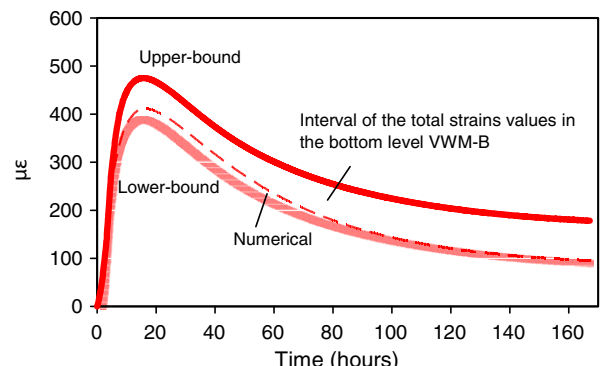


Fig. 16. Total strains  $\varepsilon_x$  at the bottom level assuming reduction of  $\alpha_T$  along hydration.

specially due to the different methodologies used to measure the thermal dilation coefficient, as it still does not exist a consensus within scientific community in this concern. In this figure it stands out that at the first 5 h (corresponding to a concrete development stage during which the role of the liquid phase is of major importance)  $\alpha_T$  assumes values around  $20 \times 10^{-6}$  [33] or even higher, decreasing for less than half with the advancement of the concrete hardening process (increasing relevance of the solid phase).

In order to evaluate the influence of the  $\alpha_T$  reduction during hydration on the early-age concrete total strains, a new thermo-mechanical numerical analysis was carried out by implementing the experimental evolution of  $\alpha_T$  reported by Bjontegaard and Sellevold [34], and depicted in Fig. 15. The corresponding numerical predictions for the concrete total strains  $\epsilon_x$  at the bottom level are depicted in Fig. 16. Now the numerical predictions are considerably more coherent with the experimental measurements, not only during the cooling phase but also during the heating phase, and it can be also observed that the numerical total strains fall within the interval of expectable strains provided by the two types of vibrating wire strain gages (with metallic and plastic casings). Relevance of explicitly including concrete  $\alpha_T$  reduction throughout the first hours of cement hydration is therefore highlighted, which calls for the urgent need of an adequate set-up to experimentally determinate this property, with a huge relevance for early-age concrete behaviour.

## 5. Conclusions

Performances of vibrating wire strain gages with casings of different stiffnesses (metallic and plastic) were evaluated through measurements on a concrete prism tested in laboratory since the instant of casting. It was shown that the plastic vibrating wire strain gage, of very low stiffness, has the advantage of sooner solidarization to concrete, but exhibits a higher thermal sensitivity in the pre-solidarization phase, when compared to the metallic vibrating wire strain gage, leading to higher total strains in the heating period. Therefore, for *in situ* monitoring works that involve early-age concrete strains it is recommended to use metallic vibrating wire strain gages, as they are more robust and present lower temperature sensitivity. However, the plastic vibrating wire strain gages are important for defining the instant of solidarization to concrete of the metallic vibrating strain gages, such instant being defined when the two types of strain gages commence to respond with similar tendencies. Furthermore, it was shown the possibility to obtain an upper-bound of the concrete total strains (coincident with the signal directly provided by the sensor), and also a lower-bound (by subtracting to the original signal the strains recorded by the metallic gage until the solidarization to concrete).

A well succeeded thermal analysis of the concrete prism was described, with the temperatures predicted numerically and the ones recorded by the sensors according fairly well. The adopted thermo-mechanical model also predicted the total strains developed in concrete during the early-ages. During the cooling period the numerical results showed coherence with the development tendencies observed in the measurements from vibrating wire strain gages. Although the maximum total strains recorded by the sensors during the heating phase were superior to the initial numerical predictions, it was demonstrated that this discrepancy was specially due to the reduction on the concrete thermal dilation coefficient that takes place during the first 5–10 h since concrete casting, a feature that usually is not considered in the numerical simulations, as it is difficult to characterize experimentally.

## Acknowledgements

Funding provided by the Portuguese Foundation for Science and Technology (FCT) to the Research Project POCI/ECM/56458/2004, as well as to the first author through the Ph.D. Grant SFRH/BD/13137/2003, is gratefully acknowledged.

## References

- [1] Faria R, Azenha M, Figueiras JA. Modelling of concrete at early ages: application to an externally restrained slab. *Cem Concr Compos* 2006;28(6):572–85.
- [2] Cusson D. Field monitoring of the early-age performance of concrete structures. In: Bentur A, editor. Early age cracking in cementitious systems, Report 25. RILEM Publications s.a.r.l.; 2002.
- [3] Anson M, Rowlinson P. Early-age strain and temperature measurements in concrete tanks. *Mag Concr Res* 1988;40(145):216–26.
- [4] Heimdal E, Kompen R. Maridal Culvert, Norway – field test I. IPACS Document, Subtask T.5.1.1; 2001.
- [5] Morabito P. Sluice gate – Brembo River – Italy – field test. IPACS Document, Subtask T.5.4; 2001.
- [6] Cervera M, Faria R, Oliver J, Prato T. Numerical modelling of concrete curing, regarding hydration and temperature phenomena. *Comput Struct* 2002;80(18–19):1511–21.
- [7] Azenha M, Faria R. Temperatures and stresses due to cement hydration on the R/C foundation of a wind tower – a case study. *Eng Struct* 2008;30(9):2392–400.
- [8] O'Moore L, Bawejah D, Cux P. Investigation of early age tensile stresses, shrinkage strains in pavements and standard drying shrinkage tests. Department of Civil Engineering – Concrete Laboratory, University of Queensland. Internal Report; 2004.
- [9] Glisic B, Simon N. Monitoring of concrete at very early age using stiff SOFO. *Cem Concr Compos* 2000;22(2):115–9.
- [10] Habel W, Hofmann D, Hillemeyer B. Deformation measurements of mortars at early ages and of large concrete components on site by means of embedded fiber-optic microstrain sensors. *Cem Concr Compos* 1997;19(1):81–102.
- [11] Slowik V, Schlattner E, Klink T. Experimental investigation into early age shrinkage of cement paste by using fibre Bragg gratings. *Cem Concr Compos* 2004;26(5):473–9.
- [12] Wong C, Childs P, Berndt R, Macken T, Peng G, Gowripalan N. Simultaneous measurement of shrinkage and temperature of reactive powder concrete at early-age using fibre Bragg grating sensors. *Cem Concr Compos* 2007;29(6):490–7.
- [13] Glisic B, Inaudi D. Monitoring of early and very early age deformation of concrete using fiber optic sensors, FIB – Fédération Internationale du Béton. In: Proceedings of the 2nd international congress, Naples, Italy; 2006.
- [14] Glisic B, Inaudi D. Structural monitoring of hybrid specimens at early age using fibre optic sensors. In: 55th Rilem Annual Week, Symp. on connections between Steel and Concrete, Stuttgart, Germany; 2001.
- [15] Azenha M. Behaviour of concrete at early ages. Phenomenology and thermo-mechanical analysis. M.Sc. Thesis, Faculty of Engineering of the University of Porto, 2004 [in Portuguese].
- [16] Reinhardt HW, Blaauwendraad J, Jongedijk J. Temperature development in concrete structures taking account of state dependent properties. In: Int. conf. concrete at early ages, Paris, France; 1982.
- [17] Carino N, Lew H. The maturity method: from theory to application, 2001. Washington (DC): Structures Congress & Exposition; 2001.
- [18] CEN. Eurocode 2: design of concrete structures – part I: general rules and rules for buildings. Brussels; 2004.
- [19] Bazant ZP. Mathematical modeling of creep and shrinkage of concrete. Chichester: John Wiley & Sons Inc.; 1988.
- [20] de Borst R, van den Boogaard AH. Finite-element modeling of deformation and cracking in early-age concrete. *J Eng Mech ASCE* 1994;120(12):2519–34.
- [21] Atrushi D. Tensile and compressive creep of early age concrete: testing and modelling. Ph.D. Thesis, Norwegian University of Science and Technology, Trondheim, Norway; 2003.
- [22] Ji G. Cracking risk of concrete structures in the hardening phase: experiments, material modeling and finite element analysis. Trondheim, Norway: Norwegian University of Science and Technology; 2008.
- [23] Bazant Z, Prasannan S. Solidification theory for concrete creep: I. Formulation. *J Eng Mech ASCE* 1989;115(8):1691–703.
- [24] Jonasson J-E. Modelling of temperature, moisture and stresses in young concrete. Ph.D. Thesis, Lulea University of Technology, Lulea; 1994.
- [25] Silva L, Faria R, Azenha M. Calorimetric characterization of cements at the hydration phase. FCT report – project POCI/ECM/56458/2004. LABEST – Faculty of Engineering of the University of Porto; 2006 [in Portuguese].
- [26] D'Aloia L, Chanvillard G. Determining the “apparent” activations energy of concrete: Ea – numerical simulations of the heat of hydration of cement. *Cem Concr Res* 2002;32(8):1277–89.
- [27] Kada H, Wirquin E, Duthoit B. Determination of the apparent activations energy of concrete by isothermal calorimetry. *Cem Concr Res* 2000;30(3):301–5.
- [28] FIB. Structural concrete – textbook on behaviour, design and performance updated knowledge of the CEB/FIP model code 1990, vol 1, FIB – CEB/FIP; 1999.

- [29] Khan A, Cook WD, Mitchell D. Thermal properties and transient thermal analysis of structural members during hydration. *ACI Mater J* 1998;95(3):293–303.
- [30] Azenha M, Magalhaes F, Faria R, Cunha A. Measurement of concrete E-modulus evolution since casting: A novel method based on ambient vibration. LABEST Internal Report; 2008.
- [31] Atrushi D, Bjontegaard O, Kanstad T, Sellevold E. Creep deformations in hardening concrete: test method investigations and the effect of temperature. IPACS Document, Subtask 3.2; 2001.
- [32] Prato T. Behaviour of concrete at early ages. Modelling and applications. Ph.D. Thesis, Universitat Politècnica de Catalunya, Barcelona; 1999 [in Spanish].
- [33] Viviani M, Glisic B, Smith I. Separation of thermal and autogenous deformation at varying temperatures using optical fiber sensors. *Cem Concr Compos* 2007;29(6):435–47.
- [34] Bjontegaard O, Sellevold E. Interaction between thermal dilation and autogenous deformation in high performance concrete. *Mater Struct* 2001;34(5):266–72.